
Correcting boundary over-exploration deficiencies in Bayesian optimization with virtual derivative sign observations

Eero Siivola¹, Aki Vehtari¹, Jarno Vanhatalo², Javier González^{3,*}

¹Aalto University, Dept. of Computer Science, {eero.siivola, aki.vehtari}@aalto.fi

²University of Helsinki, Dept. of Math. and Stat., and Dept. of Biosciences, jarno.vanhatalo@helsinki.fi

³Amazon.com, gojav@amazon.com

Abstract

Bayesian optimization (BO) is a global optimization strategy designed to find the minimum of an expensive black-box function, typically defined on a continuous subset of \mathcal{R}^d , by using a Gaussian process (GP) as a surrogate model for the objective. Although currently available acquisition functions address this goal with different degree of success, an over-exploration effect of the contour of the search space is typically observed. However, in problems like the configuration of machine learning algorithms, the function domain is conservatively large and with a high probability the global minimum does not sit the boundary. We propose a method to incorporate this knowledge into the searching process by adding virtual derivative observations in the GP at the borders of the search space. We use the properties of GPS to impose conditions on the partial derivatives of the objective. The method is applicable with any acquisition function, it is easy to use and consistently reduces the number of evaluations required to optimize the objective irrespective of the acquisition used. We illustrate the benefits our approach in an extensive experimental comparison.

1 INTRODUCTION

Global optimization is a common problem in a very broad range of applications. Formally, it is defined as finding $\mathbf{x}_{\min} \in \mathcal{X} \subset \mathcal{R}^d$ such that

$$\mathbf{x}_{\min} = \arg \min_{\mathbf{x} \in \mathcal{X}} f(\mathbf{x}), \quad (1)$$

*Work done while Javier González was at the University of Sheffield

where \mathcal{X} is generally considered to be a bounded set. In this work, we focus on cases in which f is a black-box function whose explicit form is unknown and that it is expensive to evaluate. This implies that we need to find the \mathbf{x}_{\min} with a finite, typically, small number of evaluations, which transform the original *optimization* problem in a sequence of *decision* problems.

Bayesian optimization of black-box functions using Gaussian Processes (GPS) as surrogate priors has become popular in recent years (see, e.g., review by [Shahriari et al., 2016b](#)). It has been proven to be an efficient method to treat the decision problems of where to evaluate f using statistical *inference*. This is typically done by means of an acquisition function that change after each point is collected and that balances *exploration* and *exploitation* in the search.

A common problem that has not been systematically studied in the BO literature is the tendency of most acquisition strategies to over-explore the boundary of the function domain \mathcal{X} . This issue is not relevant if the global minimum may lie on the border of the search space but in most cases, including when the search space is unbounded ([Shahriari et al., 2016a](#)), this is not the case. This effect has also been observed in the active learning literature ([Krause and Guestrin, 2007](#)) and it is known to appear when the search is done myopically, as it is the case in most acquisitions functions. Non-myopic approaches in BO ([González et al., 2016](#); [Osborne et al., 2009](#)) can potentially deal with this problem but they are typically very expensive to compute.

In this paper we propose a new approach to correct the *boundary over-exploration effect* of most acquisitions without having to assume the computational overhead of currently available non-myopic methods. We demonstrate that when the global minimum is known not to lie on the boundary of \mathcal{X} , this information can be embedded in the problem. In these cases, it holds that the gradient of the underlying function points towards the centre on

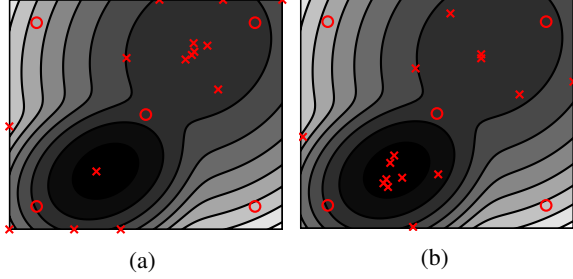


Figure 1: Sequence of 15 evaluations when optimizing a combination of Gaussians (darker colors represent lower function values) with (a) standard BO (b) and the proposal of this work. The five red circles are the points used to initialize the GP. The 15 red crosses are the acquisitions. The GP-LCB acquisition function was used in both cases (see Section 2.2 for details). With the new proposal, less evaluations are spent in the boundary, and more points are collected around the global optimum.

all borders. This property can be used by including additional prior information about the shape of the function by means of virtual derivative observations. In other words, we use non-observed partial derivative data to support our prior assumption about the shape of the underlying function (its gradients on the boundary of the domain). As the derivative of a GP is also a GP (O'Hagan, 1992), including virtual derivative observations in GPs is feasible with standard inference methods. As it is shown in this work, this reduces the number of required function evaluations giving rise to a battery of more efficient BO methods.

The unwanted boundary over-exploration effect of the regular BO is illustrated in Figure 1 (a). A simple function consisting of two Gaussian components is optimized with the standard BO and the proposal of this work. The correction of the over-exploration effect is evident.

1.1 Related Work

Derivative observations have been used before in the BO and GP context. Koistinen et al. (2016, 2017) use Gaussian processes with derivative observations for Bayesian optimization (BO) of minimum energy path transitions of atomic rearrangements and Wu et al. (2017) use derivative observations to decrease the number of observations needed for finding the function optimum.

Derivative observations can be used to provide shape priors. To constrain a function to have a mode in a specified location Gosling et al. (2007) add virtual observations of first derivative being zero and the second derivative being negative. Riihimäki and Vehtari (2010) use virtual derivative observations, where only the sign of the derivative is

known, to add monotonicity information. Jauch and Peña (2016) use in similar way virtual derivative observations for convexity and quasi-convexity constraints. To handle inference for the non-Gaussian contribution of the derivative sign information, Gosling et al. (2007), Riihimäki and Vehtari (2014), and Jauch and Peña (2016) use rejection sampling, Riihimäki and Vehtari (2010) use expectation propagation (EP), and Wang and Berger (2016) use Markov chain Monte Carlo (MCMC). Unlike rejection and projection based shape constraints, monotonicity via virtual observations scales moderately well with a number of dimensions as shown by Riihimäki and Vehtari (2010) and Siivola et al. (2016).

Surprisingly, over-exploration of boundaries has not been systematically studied before. A naive approach is to use a quadratic mean function to penalize the search in the boundary. However, this has strong limitations when the optimized function is multimodal or far away from being quadratic as demonstrated in Riihimäki and Vehtari (2010).

1.2 Contributions

The main contributions of this work are:

- A new approach for Bayesian optimization that corrects the over-exploration of the boundary of most acquisitions. The method is simple to use, can be combined with any acquisitions and always work equally or better than the standard approach. After a review of the needed background, the method is described in Section 3.
- A publicly available code framework available at [to be disclosed after publication] that contains an efficient implementation of the methods described in this work
- An exhaustive analysis of the performance of the proposed method in a variety of scenarios that should give the reader a precise idea about the (i) the loss in efficiency incurred in standard methods due to the boundary over-exploration and (ii) how this issue is significantly relieved with our proposal.

In addition to the previous points Section 5 contains a discussion of future directions and the main lessons learned in this work.

2 BACKGROUND AND PROBLEM SET-UP

The main iterative steps of any BO algorithm are: (i) Model the objective function with GP prior, which is up-

dated with the selected evaluations so far. (ii) Use an acquisition function, that depends on the posterior for the objective function, to decide what the next query point should be. Next, we briefly visit both of them and detail how information from derivative observations can be naturally incorporated in the loop.

2.1 Standard GP Surrogate for Modeling of f

At iteration $n + 1$, we assume that we have evaluated the objective function n times providing us the data $\mathbf{D} = \{y^{(i)}, \mathbf{x}^{(i)}\}_{i=1}^n$ where $y^{(i)}$ is, the possibly noisy, function evaluation at input location $\mathbf{x}^{(i)}$. To combine our previous knowledge about f with the dataset \mathbf{D} , we use a GP to model. In particular, a GP prior is directly specified on the latent function with prior assumptions encoded in the covariance function $k(\mathbf{x}^{(1)}, \mathbf{x}^{(2)})$, which specifies the covariance of two latent function values $f(\mathbf{x}^{(1)})$ and $f(\mathbf{x}^{(2)})$. A zero mean Gaussian process prior

$$p(\mathbf{f}) = N(\mathbf{f} | \mathbf{0}, \mathbf{K}), \quad (2)$$

is chosen, where \mathbf{K} is a covariance matrix between n latent values \mathbf{f} at input used for training, $\mathbf{X} = (\mathbf{x}^{(1)}, \dots, \mathbf{x}^{(n)})$, s.t. $\mathbf{K}_{ij} = k(\mathbf{x}^{(i)}, \mathbf{x}^{(j)})$.

In regression, n noisy observations \mathbf{y} and o latent function values \mathbf{f}_* at the test inputs \mathbf{X}_* are assumed to have Gaussian relationship. With the noise variance σ^2 , the covariance between the latent values at the training and test inputs \mathbf{K}_* , the covariance matrix of the latent values at the test inputs \mathbf{K}_{**} and n dimensional identity matrix \mathbf{I} , the joint distribution of the observations and latent values at the test inputs is

$$\begin{bmatrix} \mathbf{y} \\ \mathbf{f}_* \end{bmatrix} \sim N\left(\mathbf{0}, \begin{bmatrix} \mathbf{K} + \sigma^2 \mathbf{I} & \mathbf{K}_*^T \\ \mathbf{K}_* & \mathbf{K}_{**} \end{bmatrix}\right). \quad (3)$$

Using the Gaussian conditioning rule, the predictive distribution becomes $\mathbf{f}_* | \mathbf{y} \sim N(\boldsymbol{\mu}_*, \boldsymbol{\Sigma}_*)$ with

$$\begin{aligned} \boldsymbol{\mu}_* &= \mathbf{K}_* (\mathbf{K} + \sigma^2 \mathbf{I})^{-1} \mathbf{y}, \\ \boldsymbol{\Sigma}_* &= \mathbf{K}_{**} - \mathbf{K}_* (\mathbf{K} + \sigma^2 \mathbf{I})^{-1} \mathbf{K}_*^T. \end{aligned}$$

so the predictive distribution of the GP can be written explicitly for any point in the domain.

2.2 Acquisition Policies

Among others, some very well established acquisition functions are available. The *expected Improvement* (EI) maximizes the expected gain over the current best (Jones et al., 1998). The *lower confidence bound* (LCB) minimizes the regret over the optimization area (Srinivas et al., 2010) Brochu E., Cora V. M., and de Freitas N. (2010).

The *probability of improvement* (MPI), selects the next point where probability of improving over the current best is the highest (Kushner, 1964). Although these are some of the most widely used acquisition functions, they all suffer from the over exploration effect described in the introduction of this work. As we will detail later, the ability of GPs to handle derivative observations will be key to correct this effect. Next, we revisit the main elements to incorporate gradient information in the GPs before we detail the specifics of our proposal.

2.3 Incorporating Partial Derivative Observations in the Loop

Since the differentiation is a linear operator, the partial derivative of a Gaussian process remains a Gaussian process (Solak et al., 2003; Rasmussen and Williams, 2006). Thus, using partial derivative values for prediction and making predictions about the partial derivatives at a given point is easy to incorporate in the model and therefore in the BO search. Since

$$\begin{aligned} \text{cov}\left(\frac{\partial f^{(i)}}{\partial x_g^{(i)}}, f^{(j)}\right) &= \frac{\partial}{\partial x_g^{(i)}} \text{cov}(f^{(i)}, f^{(j)}), \\ \text{cov}\left(\frac{\partial f^{(i)}}{\partial x_g^{(i)}}, \frac{\partial f^{(j)}}{\partial x_h^{(j)}}\right) &= \frac{\partial^2}{\partial x_g^{(i)} \partial x_h^{(j)}} \text{cov}(f^{(i)}, f^{(j)}) \end{aligned}$$

covariance matrices in Equations (2) and (3) can be extended to include partial derivatives either as observations or as values to be predicted.

Following Riihimäki and Vehtari (2010), denote by m the partial derivative value in the dimension j at $\tilde{\mathbf{x}}$. Then the probability of observing partial derivative is modelled using probit likelihood with a control parameter ν (see details in Riihimäki and Vehtari, 2010)

$$p\left(m \mid \frac{\partial \tilde{f}}{\partial \tilde{x}_j}\right) = \Phi\left(\frac{\partial \tilde{f}}{\partial \tilde{x}_j} \frac{1}{\nu}\right), \quad (4)$$

where

$$\Phi(z) = \int_{-\infty}^z N(t | 0, 1) dt.$$

Let \mathbf{m} be a vector of q partial derivative values at $\tilde{\mathbf{X}} = (\tilde{\mathbf{x}}^{(1)}, \dots, \tilde{\mathbf{x}}^{(q)})$, \mathbf{j} be a vector of the dimensions of the partial derivatives and $\tilde{\mathbf{f}}$ be the vector of latent values at $\tilde{\mathbf{X}}$. For shorthand, let the partial derivatives of latent values be

$$\tilde{\mathbf{f}}' = \left(\frac{\partial \tilde{f}^{(1)}}{\partial \tilde{x}_{j^{(1)}}^{(1)}}, \dots, \frac{\partial \tilde{f}^{(q)}}{\partial \tilde{x}_{j^{(q)}}^{(q)}} \right).$$

Assuming conditional independence given the latent

derivative values, the likelihood becomes

$$p(\mathbf{m} \mid \tilde{\mathbf{f}}') = \prod_{i=1}^q \Phi \left(\frac{\partial \tilde{\mathbf{f}}^{(i)}}{\partial \tilde{\mathbf{x}}_{j^{(i)}}^{(i)}} \frac{1}{\nu} \right).$$

With function values at \mathbf{X} and partial derivative values at $\tilde{\mathbf{X}}$, the joint prior for \mathbf{f} and $\tilde{\mathbf{f}}$ then becomes

$$p \left(\begin{bmatrix} \mathbf{f} \\ \tilde{\mathbf{f}}' \end{bmatrix} \mid \begin{bmatrix} \mathbf{X} \\ \tilde{\mathbf{X}} \end{bmatrix} \right) = \mathcal{N} \left(\begin{bmatrix} \mathbf{f} \\ \tilde{\mathbf{f}}' \end{bmatrix} \mid \mathbf{0}, \begin{bmatrix} \mathbf{K}_{\mathbf{f}, \mathbf{f}} & \mathbf{K}_{\mathbf{f}, \tilde{\mathbf{f}}'} \\ \mathbf{K}_{\tilde{\mathbf{f}}', \mathbf{f}} & \mathbf{K}_{\tilde{\mathbf{f}}', \tilde{\mathbf{f}}'} \end{bmatrix} \right).$$

The joint posterior for the latent values and the latent value derivatives can be derived from the Bayes' rule

$$p(\mathbf{f}, \tilde{\mathbf{f}}' \mid \mathbf{y}, \mathbf{m}, \mathbf{X}, \tilde{\mathbf{X}}) = \frac{p(\mathbf{f}, \tilde{\mathbf{f}}' \mid \mathbf{X}, \tilde{\mathbf{X}}) p(\mathbf{y} \mid \mathbf{f}) p(\mathbf{m} \mid \tilde{\mathbf{f}}')}{Z}, \quad (5)$$

with $Z = \int p(\mathbf{f}, \tilde{\mathbf{f}}' \mid \mathbf{X}, \tilde{\mathbf{X}}) p(\mathbf{y} \mid \mathbf{f}) p(\mathbf{m} \mid \tilde{\mathbf{f}}') d\mathbf{f} d\tilde{\mathbf{f}}'$. Note that since $p(\mathbf{m} \mid \tilde{\mathbf{f}}')$ is not Gaussian, the full posterior is analytically intractable and some approximation method must be used. Following [Riihimäki and Vehtari \(2010\)](#), we use expectation propagation (EP) for fast and accurate approximative inference.

Model comparison is often done with the energy function, or negative log marginal posterior likelihood of the data

$$E(\mathbf{y}, \mathbf{m} \mid \mathbf{X}, \tilde{\mathbf{X}}) = -\log p(\mathbf{y}, \mathbf{m} \mid \mathbf{X}, \tilde{\mathbf{X}}).$$

If we are interested in only some part of the model, selected points $\{\mathbf{y}^*, \mathbf{X}^*\}$ can be used to evaluate the model fit

$$\begin{aligned} E(\mathbf{y}^* \mid \mathbf{X}^*, \mathbf{y}, \mathbf{m}, \mathbf{X}, \tilde{\mathbf{X}}) &= -\log p(\mathbf{y}^* \mid \mathbf{X}^*, \mathbf{y}, \mathbf{m}, \mathbf{X}, \tilde{\mathbf{X}}) \\ &= -\log \frac{p(\mathbf{y}^*, \mathbf{y}, \mathbf{m} \mid \mathbf{X}^*, \mathbf{X}, \tilde{\mathbf{X}})}{p(\mathbf{y}, \mathbf{m} \mid \mathbf{X}, \tilde{\mathbf{X}})}. \end{aligned} \quad (6)$$

Depending on the choice of covariance function, GPS have various amount of parameters that must be selected. These hyperparameters include also the noise variance of the assumed Gaussian relationship between the observations and latent values. This topic of hyperparameter optimization is not covered here but the reader is further advised to see, for example, [Rasmussen and Williams \(2006\)](#) and [Snoek et al. \(2012\)](#).

3 BAYESIAN OPTIMIZATION WITH VIRTUAL DERIVATIVE SIGN OBSERVATIONS

In this section we illustrate how, virtual derivative observations can be added to the edges of the search space. In essence, the model used is the same one described in

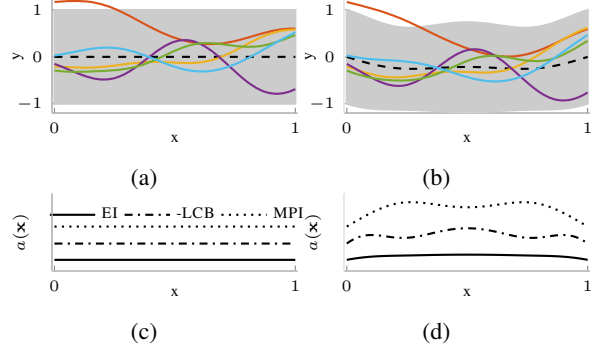


Figure 2: The GP prior in BO visualized (a) without virtual derivative observations, (b) with virtual derivative observations on both borders. Black dotted line is the mean of the GP, the light gray area is 68% central posterior interval and the five lines represent random function samples drawn from the prior. The acquisitions function values as a function of x are visualized for GPS (c) without virtual derivative observations, (d) with virtual derivative observations on both borders, for all three acquisition functions EI, LCB and MPI. Since the next acquisition is chosen as maximum of EI and MPI, but as a minimum of LCB, LCB is plotted as -LCB in order for the curves to be easily comparable.

Section 2.3 but where observed derivative observations are replaced by 'virtual' ones at the boundaries of the domain to correct the previously described over-exploration effect.

3.1 Virtual Derivative-Based Search

To encode the prior knowledge of the non-border minimum to the optimization algorithm, we propose the following dynamic approach. Just like in the regular BO with GP prior presented in the Section 2, the objective function is given a GP prior which is updated according to the objective function evaluations so far. The next evaluation point is the acquisition function maximum, but if it is closer than threshold ϵ_b to the border of the search space, the point is projected to the border and a virtual derivative observation is placed to that point instead. After having added this virtual observation, the GP prior is updated and new proposal for the next acquisition is computed. In theory we could add virtual observations statically to the borders before starting the optimization, but to reduce the computational cost we use lazy addition of the virtual observations only when and where it is needed. Algorithm 1 contains pseudo code for the proposed method.

Since there is no actual knowledge about the true value of the partial derivatives on the borders, posterior distribution should behave robustly to deviations in the actual partial derivative values. By using ν very close to zero

Algorithm 1 Pseudo code of the proposed BO method. The inputs are the acquisition a , the *stopping criterion* and the GP model. Note that this algorithm reduces to standard BO when lines 4-6 are removed.

```

1: while stopping criterion is False do
2:   Fit GP to the available dataset  $\mathbf{X}, \mathbf{y}$ .
3:   Optimise acquisition function,  $a$ , to find select new
   location  $\mathbf{x}$  to evaluate.
4:   if  $\mathbf{x}$  is close to the edge then
5:     Augment  $\mathbf{X}$  with a virtual derivative sign obser-
     vation at  $\tilde{\mathbf{x}}$ .
6:   else
7:     Augment  $\mathbf{X}$  with  $\mathbf{x}$  and evaluate  $g$  at  $\mathbf{x}$ .
8:   end if
9: end while

```

in Equation (4), the probit likelihood becomes very steep. This means that the likelihood values are close to 1 for all partial derivative values $m > 0$ and close to zero for all $m < 0$. Thus the assumed numeric partial derivative values do not matter and for instance $m_{d_i}^{(i)} = \pm 1$ can be used to express prior information on the borders. The effect of adding a virtual derivative observations on the borders of one dimensional function is visualized in the Figure 2. From the Figure it can be seen that the virtual derivative observations alter both the GP prior and the acquisition functions to resemble our prior belief of the location of the minimum.

Another parameter to be chosen is the threshold ϵ_b . As acquisitions closer than threshold are always rejected, ϵ_b should not be too large. Another argument to avoid too large values is the fading information value of the virtual observations. If the GP allows rapid changes in the latent values, virtual derivative observations affect the posterior distribution only very locally and the added observations might affect to the posterior distribution only very marginally. However, if the threshold is too small, virtual observations are added very seldom and the algorithm differs only a little from the standard BO. Let l be the diameter of the search space. Our experiments suggest that $\epsilon_b \approx 0.01 \cdot l$ provides a good trade-off for adaptivity.

Basic time complexity of GP is $\mathcal{O}((n+q)^3)$, where n is the number of training samples and q is the number of partial derivative observations. If the search space is restricted to be a hyper-cube, partial derivative only in one direction is needed when a virtual observation is added on the edge of the search space, which helps to keep the number of partial derivative observations relatively small. Naturally various sparse approximations could be used to improve the scaling of the GP computation, but here we focus on problems where we assume that acquisitions are costly and n is moderate. Thus, the time complexity of

the algorithm itself is negligible compared to the time of acquisitions.

3.2 Adaptive Search

For some practical applications, the presented algorithm might make too strict assumptions about the underlying function not having minima at the borders. Especially with functions having multiple minima, local minima might be on the border. For better local accuracy, the following modifications to Algorithm 1 can be used.

Before placing a virtual derivative observation on the border, it can be checked whether or not the existing data supports the virtual gradient sign observation to be added to the model. This can be done by checking the energy values (Equation (6)) of virtual observations of different directions, $m_{d_i}^{(i)} \in \{-1, 1\}$. Since the probit likelihood (4) is close to step function, energy function values can be used to approximate posterior probability of derivative sign, (e.g. $p(m_{d_i}^{(i)} > 0 | \mathbf{x}^*, \mathbf{y}, \mathbf{m}, \mathbf{X}, \tilde{\mathbf{X}})$). If the energy of the assumed derivative sign is smaller than of opposite direction, it is reasonable to add the virtual observation.

Since virtual gradient observations tell only the direction of the gradient, they do not affect as much to the uncertainty of a GP as regular observations. As a result, if there are minima on border, acquisitions might be proposed to locations where already exists virtual observations. If this happens, it is reasonable to remove the virtual observation before adding the new acquisition.

4 EXPERIMENTS

In this section we introduce the four case studies performed to gain insight about the performance of the proposed method. First the details of the experiments are presented and then each study and its results are presented.

4.1 Experimental Set-Up

The proposed Bayesian optimization algorithm was implemented in GPy toolbox¹. In all case studies to be covered later, we use zero mean GP prior for regular observations and probit likelihood with scaling parameter $\nu = 10^{-6}$ for the virtual derivative observations. In addition to this, we use the squared exponential covariance function,

$$k(\mathbf{x}, \mathbf{x}') = \sigma_f^2 \exp \left\{ -\frac{1}{2} \sum_{i=1}^d \frac{(\mathbf{x}_i - \mathbf{x}'_i)^2}{l^2} \right\},$$

¹Toolbox available at: <https://sheffieldml.github.io/GPy/>

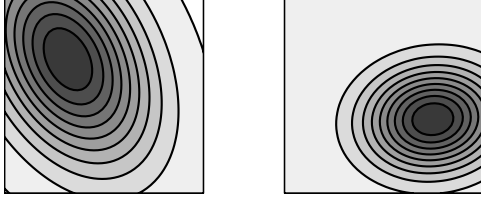


Figure 3: Two examples of two dimensional random normal distribution functions. In both examples, the figure bounds represent the search space, darker areas represent lower function values.

where d is the input space size, σ_f^2 is magnitude and l is characteristic length scale. The partial derivatives are

$$\begin{aligned} \frac{\partial k(\mathbf{x}, \mathbf{x}')}{\partial \mathbf{x}_j} &= -\sigma_f^2 \exp \left\{ -\frac{1}{2} \sum_{i=1}^d \frac{(\mathbf{x}_i - \mathbf{x}'_i)^2}{l^2} \right\} \\ &\quad \times \frac{\mathbf{x}_j - \mathbf{x}'_j}{l^2}, \\ \frac{\partial k(\mathbf{x}, \mathbf{x}')}{\partial \mathbf{x}'_j} &= -\frac{\partial k(\mathbf{x}, \mathbf{x}')}{\partial \mathbf{x}_j}, \\ \frac{\partial k(\mathbf{x}, \mathbf{x}')}{\partial \mathbf{x}_j \mathbf{x}'_k} &= \sigma_f^2 \exp \left\{ -\frac{1}{2} \sum_{i=1}^d \frac{(\mathbf{x}_i - \mathbf{x}'_i)^2}{l^2} \right\} \\ &\quad \times \left(-\frac{\mathbf{x}_j - \mathbf{x}'_j}{l^2} \frac{\mathbf{x}_k - \mathbf{x}'_k}{l^2} + \frac{\delta_{jk}}{l^2} \right), \end{aligned}$$

which are needed to compute the virtual derivatives.

Initial acquisitions are generated with full factorial design (Croarkin et al., 2013). In the experiments, we use 2^d points to initialize the GP (see 5.3.3.3. from the citation).

Three BO algorithms are used in the case studies. Standard BO algorithm (referred as vanilla BO, VBO), BO algorithm with virtual derivative sign observations (referred as derivative BO, DBO) and adaptive version of DBO (referred as ADBO). For the last two of these, virtual derivative sign observations are added if the next proposed point is within 1% of the length of the edge of the search space to any border. For ADBO, old virtual derivative observations are removed before adding regular observation if the euclidean distance between the points is less than 1% of the length of the edge of the search space.

4.2 Case Study 1: A Simple Example Function

The algorithm is used to illustrate the unwanted boundary over-exploration effect of the regular BO. To show this, simple function consisting of two Gaussian components is optimized with VBO and DBO using LCB as an acquisition function. The function and 15 first acquisitions are visualized in Figure 1, in the introduction.

The results show that VBO has sampled seven points, and the proposed method has sampled four points from near the borders. Furthermore, VBO has only one acquisition from near the true minimum, whereas DBO has eight acquisitions.

4.3 Case Study 2: Random Multivariate Normal Distribution Functions

The algorithms are used to find the minimum of different d -dimensional multivariate normal distribution (MND) functions:

$$g(\mathbf{x}) = -\exp \left\{ -\frac{1}{2}(\mathbf{x} - \boldsymbol{\mu})^T \boldsymbol{\Sigma}^{-1}(\mathbf{x} - \boldsymbol{\mu}) \right\},$$

where the means $\boldsymbol{\mu}$ are selected uniformly at random such that $0.2 \leq \mu_i \leq 0.8 \forall i = 1, \dots, d$, covariances $\boldsymbol{\Sigma}$ are a random positive semidefinite matrices which eigenvalues \mathbf{e} are selected uniformly at random such that $\frac{d}{250} \leq \mathbf{e}_i \leq \frac{d}{25} \forall i = 1, \dots, d$. To simulate real life observations, random noise $\epsilon \sim N(0, s)$ is added to the observations $y(\mathbf{x}) = g(\mathbf{x}) + \epsilon$, for some fixed s . Two example functions, without noise, are visualized in Figure 3.

We drew 100 MND functions in each dimension as $d = 1, \dots, 4$, for three different noises $s = \{0, 0.05, 0.1\}$. For all these 400 functions, we ran 35 iterations for the three BO algorithms for all three acquisition functions, EI, LCB and MPI. 25, 50, and 75 percentiles of found minimum values of these functions as a function of iterations are illustrated in Figure 4 for all acquisition functions with $s = 0.1$. The Figure only displays each optimization run until it converges to the minimum. Results for other noise levels can be found from supplementary material.

The results show that in all dimensions for all acquisition functions, performances of DBO and ADBO are better than or equal to the performance of VBO. Particularly with acquisition functions EI and LCB, DBO converges to the global minimum significantly faster than VBO, especially if the function is corrupted by noise. The performance difference between ADBO and VBO is not as big, but still existing. The results also show that the variance of the optimization performance between different optimization runs is notably smaller for DBO and ADBO than for VBO.

The results can better be understood from the known properties of the presented acquisition functions. LCB is known to be most exploratory and thus it samples most acquisitions from the borders of the search space. As the presented algorithms prevent this, more acquisitions are taken further from the borders forcing the optimization towards the real minimum. The same reason also explains why the DBO and ADBO results are better if the function is corrupted by noise, as with noisy functions the

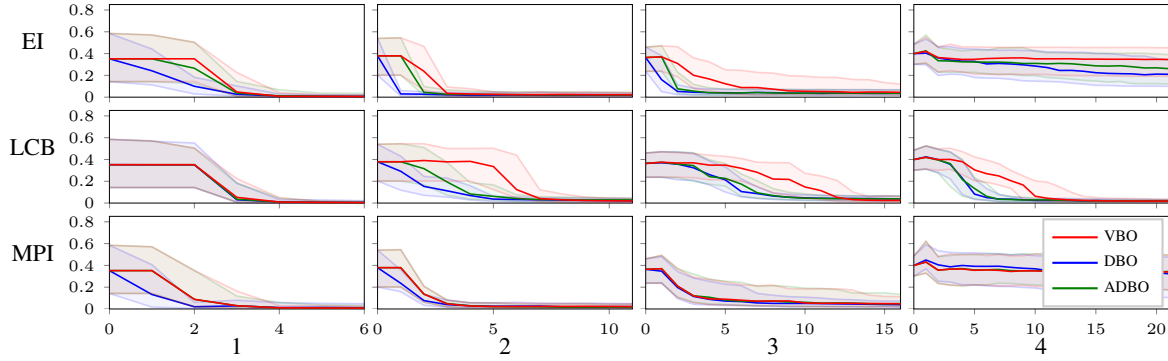


Figure 4: Each figure contains 25, 50, and 75 percentiles of found minimum of 100 optimization runs as a function of iterations for VBO, DBO and ADBO. Optimization runs are performed for MND-functions with additive noise of level $s = 0.1$. Each of the plot grids row illustrates results for different acquisition functions and each column illustrates functions of different dimension.

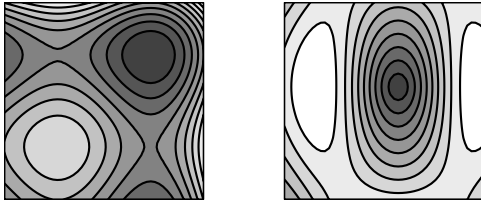


Figure 5: Two examples of two dimensional functions from the Sigopt function library. In both examples, the plot bounds represent the search space, darker areas represent lower function values.

uncertainty increases near the borders resulting to even more acquisitions there. Another interesting phenomenon in the results is illustrated with 4 dimensional functions for EI and MPI and for $s = 0.05$ and $s = 0.1$. For these acquisition functions, the latent GP function fails to model the underlying function and does not converge to the minimum. This problem is common with BO that is initialised with small amount of samples.

4.4 Case Study 3: Sigopt Function Library

Dewancker et al. (2016) introduced a benchmark function library² called Sigopt for evaluating BO algorithms. This library consists of functions of varying dimensionality and each of which belonging to one or more groups like unimodal, discrete or oscillatory functions. In addition to the functions, the library also defines the search space and true minimum of these functions. When restricting the functions to at maximum 4 dimension and taking into account only unimodal, non-discrete functions with no global border minima or large plateaus, the library

outputs 48 functions. For these functions, the number of functions per dimension varies between 10 and 14. As in the previous case study, to mimic real use cases, the function observations are corrupted with additive random noise $y(\mathbf{x}) \sim g(\mathbf{x}) + N(0, s^2)$, for $s = \{0, 0.05, 0.1\}$. Two example functions, without noise, are visualized in Figure 5.

Similarly as in the previous example, for all these functions from Sigopt dataset, we ran 35 iterations for the proposed and baseline methods for all acquisition functions. 25, 50, and 75 percentiles of found minimum values of these functions as a function of iterations are illustrated in Figure 6 for all acquisition functions with $s = 0.1$. The Figure only displays each optimization run until it converges to the minimum. Results for other noise levels can be found from supplementary material.

The results are similar as for MND functions. DBO and ADBO still perform better than VBO, especially with LCB and EI. There is not as much difference between ADBO and VBO as before. Similarly as before, the variance of the optimization performance between different optimization runs is notably smaller for DBO and ADBO than for VBO. Since there are less functions per dimension, the overall variability in the results is bigger and the percentile curves are not as smooth.

4.5 Case Study 4: Simple Gaussian Functions With Minima on Border

The algorithms are used to find minimum of similar Gaussian functions as in Section 5, with the difference that the global minima of each function is exactly on the border of the search space. Otherwise, the shape of the functions is similar as illustrated in Figure 3. The purpose of this case study is to show what happens to the performance of the

²Function library available at: <https://github.com/sigopt/evalset>

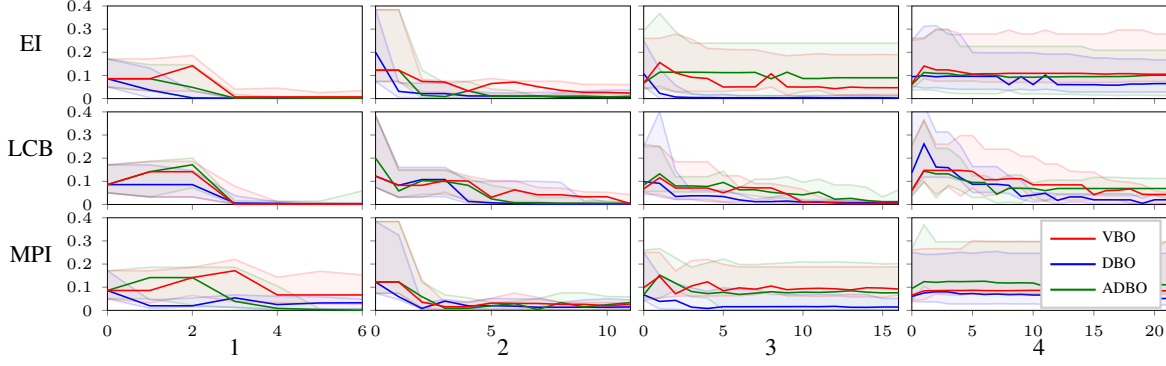


Figure 6: Same as in Figure 4, but with functions from Sigopt-library.

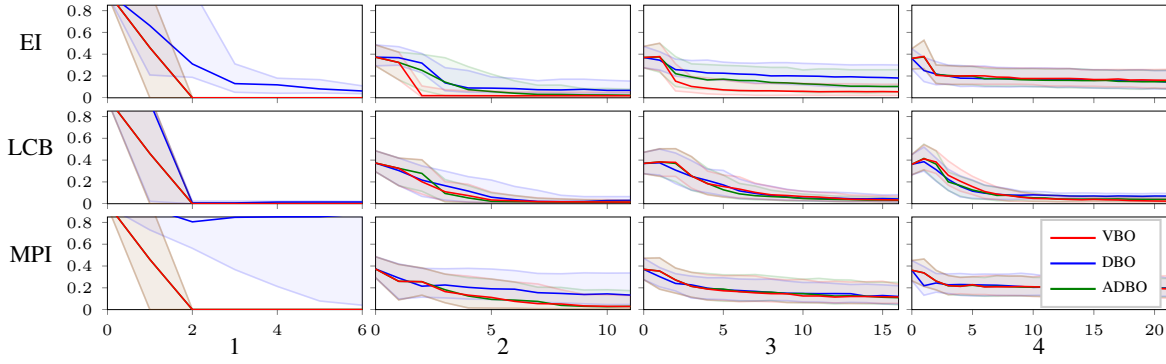


Figure 7: Same as in Figure 4, but with MND-functions that have local minimum on the edge of the search space.

proposed method if the a priori assumption is violated.

We drew 100 MND functions in each dimension as $d = 1, \dots, 4$, for three different noises $s = \{0, 0.05, 0.1\}$. For all these 400 functions, we ran 35 iterations for the three BO algorithms for all three acquisition functions, EI, LCB and MPI. 25, 50 and 75 percentiles of found minimum values of these functions as a function of iterations are illustrated in Figure 7 for all acquisition functions with $s = 0.1$. The Figure only displays each optimization run until it converges to the minimum. Results for other noise levels can be found from supplementary material.

As expected, the results show that DBO does not perform as well as VBO and ADBO. The performances of ADBO and VBO are very similar for all noise levels and dimensions for LCB and MPI, for EI it performs similar as DBO. It is surprising that for LCB, DBO performs as well as VBO.

5 CONCLUSIONS

We have presented here a Bayesian optimization algorithm which utilizes qualitative prior information concerning the objective function on the borders. Namely,

we assume that the gradient of the underlying function points towards the centre on all borders. Typical uses of Bayesian optimization concern expensive functions and in many applications qualitative knowledge of the generic properties of the function are known prior to optimization. Our approach generalizes naturally to these settings so that the user could inform the GP prior about the direction of gradient at any location of the search space.

The proposed BO method has proved to significantly improve the optimization speed and the found minimum when comparing the average performance to the performance of the standard BO algorithm without virtual derivative sign observations. The difference in performance is more significant if the assumption of non-existent global or local minima on the border of the search space holds, but is still notable if the assumption is relaxed so that the global minimum is not located on the border.

Acknowledgments

We thank Michael Andersen and Juho Piironen for their valuable comments to improve the manuscript. We also acknowledge the computational resources provided by Aalto University's Department of Computer Science.

References

Brochu E., Cora V. M., and de Freitas N. (2010). A tutorial on Bayesian optimization of expensive cost functions, with application to active user modeling and hierarchical reinforcement learning. *arXiv preprint arXiv:1012.2599*. 3

Croarkin, C., Tobias, P., and Zey, C. (2013). *Engineering statistics handbook*. NIST iTL. 6

Dewancker, I., McCourt, M., Clark, S., Hayes, P., Johnson, A., and Ke, G. (2016). A stratified analysis of Bayesian optimization methods. *arXiv preprint arXiv:1603.09441*. 7

González, J., Osborne, M. A., and Lawrence, N. D. (2016). GLASSES: relieving the myopia of Bayesian optimisation. In *Proceedings of the 19th International Conference on Artificial Intelligence and Statistics, AISTATS 2016, Cadiz, Spain, May 9-11, 2016*, pages 790–799. 1

Gosling, J. P., Oakley, J. E., and O'Hagan, A. (2007). Nonparametric elicitation for heavy-tailed prior distributions. *Bayesian Analysis*, 2(4):693–718. 2

Jauch, M. and Peña, V. (2016). Bayesian optimization with shape constraints. *arXiv preprint arXiv:1612.08915*. 2

Jones, D. R., Schonlau, M., and Welch, W. J. (1998). Efficient global optimization of expensive black-box functions. *Journal of Global Optimization*, 13(4):455–492. 3

Koistinen, O., Maras, E., Vehtari, A., and Jónsson, H. (2016). Minimum energy path calculations with Gaussian process regression. *Nanosystems: Physics, Chemistry, Mathematics*, 7(6):925–935. 2

Koistinen, O.-P., Dagbjartsdóttir, F. B., Ásgeirsson, V., Vehtari, A., and Jónsson, H. (2017). Nudged elastic band calculations accelerated with gaussian process regression. *Journal of Chemical Physics*, 147(152720). 2

Krause, A. and Guestrin, C. (2007). Nonmyopic active learning of Gaussian processes: an exploration-exploitation approach. In *Proceedings of the 24th International Conference on Machine Learning*, volume 227 of *ACM International Conference Proceeding Series*, pages 449–456. ACM. 1

Kushner, H. J. (1964). A new method of locating the maximum point of an arbitrary multipeak curve in the presence of noise. *Journal of Basic Engineering*, 86(1):97–106. 3

O'Hagan, A. (1992). Some Bayesian numerical analysis. In Bernardo, J. M., Berger, J. O., Dawid, A. P., and Smith, A. F. M., editors, *Bayesian statistics 4*, pages 345–363. Oxford University Press. 2

Osborne, M. A., Garnett, R., and Roberts, S. J. (2009). Gaussian processes for global optimization. In *3rd international conference on learning and intelligent optimization (LION3)*, pages 1–15. 1

Rasmussen, C. E. and Williams, C. K. I. (2006). Gaussian processes for machine learning. *The MIT Press*, 2(3):4. 3, 4

Riihimäki, J. and Vehtari, A. (2010). Gaussian processes with monotonicity information. In *Proceedings of the 13th International Conference on Artificial Intelligence and Statistics*, pages 645–652. 2, 3, 4

Riihimäki, J. and Vehtari, A. (2014). Laplace approximation for logistic Gaussian process density estimation and regression. *Bayesian Analysis*, 9(2):425–448. 2

Shahriari, B., Bouchard-Côté, A., and de Freitas, N. (2016a). Unbounded Bayesian optimization via regularization. In *Proceedings of the 19th International Conference on Artificial Intelligence and Statistics*, pages 1168–1176. 1

Shahriari, B., Swersky, K., Wang, Z., Adams, R. P., and de Freitas, N. (2016b). Taking the human out of the loop: A review of Bayesian optimization. *Proceedings of the IEEE*, 104(1):148–175. 1

Siivila, E., Piironen, J., and Vehtari, A. (2016). Automatic monotonicity detection for Gaussian processes. *arXiv preprint arXiv:1610.05440*. 2

Snoek, J., Larochelle, H., and Adams, R. P. (2012). Practical Bayesian optimization of machine learning algorithms. In *Advances in Neural Information Processing Systems*, pages 2951–2959. 4

Solak, E., Murray, S. R., Leithead, W. E., Leith, D. J., and Rasmussen, C. E. (2003). Derivative observations in Gaussian process models of dynamic systems. In *Advances in Neural Information Processing Systems*, pages 1033–1040. 3

Srinivas, N., Krause, A., Kakade, S. M., and Seeger, M. (2010). Gaussian process optimization in the bandit setting: No regret and experimental design. *Proceedings of the 27th International Conference on Machine Learning*. 3

Wang, X. and Berger, J. O. (2016). Estimating shape constrained functions using Gaussian processes. *SIAM/ASA Journal on Uncertainty Quantification*, 4(1):1–25. 2

Wu, J., Poloczek, M., Wilson, A. G., and Frazier, P. I. (2017). Bayesian optimization with gradients. *arXiv preprint arXiv:1703.04389*. 2

Supplementary material

Case Study 2: Random Multivariate Normal Distribution Functions

Figures 8 and 9 illustrate the results for $s = 0$ and $s = 0.05$ introduced in the Section 4.2 of the main document.

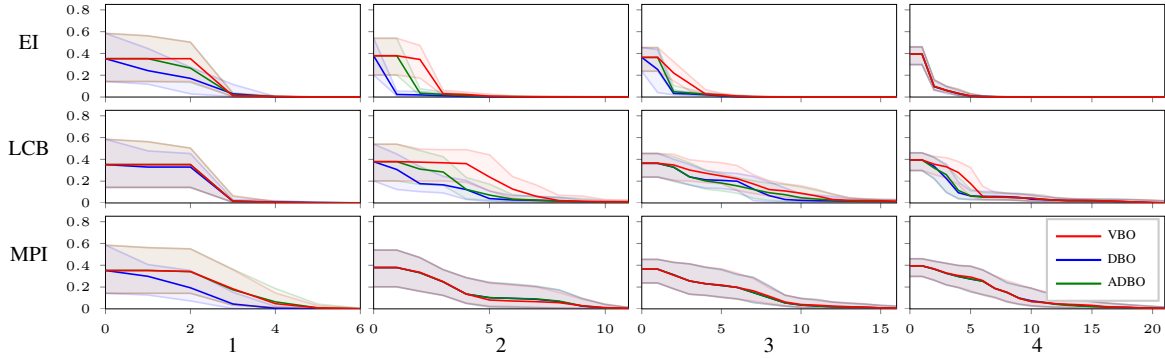


Figure 8: Each figure contains 25, 50, and 75 percentiles of found minimum of 100 optimization runs as a function of iterations for VBO, DBO and ADBO. Optimization runs are performed for MND-functions. Each of the plot grids row illustrates results for different acquisition functions and each column illustrates functions of different dimension.

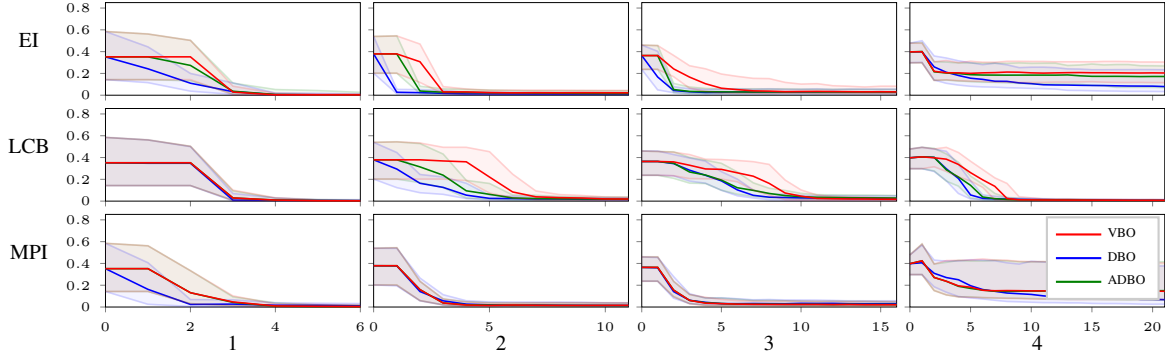


Figure 9: Same as in Figure 8, but MND-functions are corrupted with noise of level $s = 0.05$.

Case Study 3: Sigopt Function Library

Figures 10 and 11 illustrate the results for $s = 0$ and $s = 0.05$ introduced in the Section 4.3 of the main document.

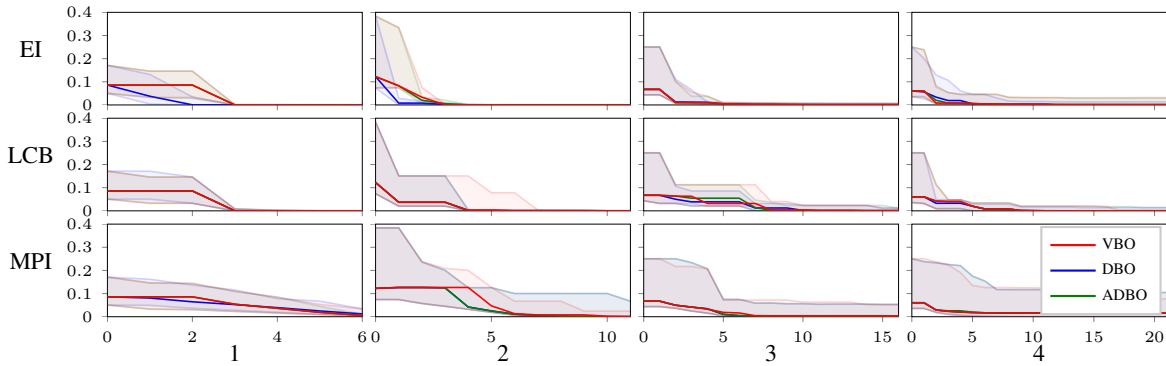


Figure 10: Same as in Figure 8 in supplementary material, but with functions from Sigopt-library.

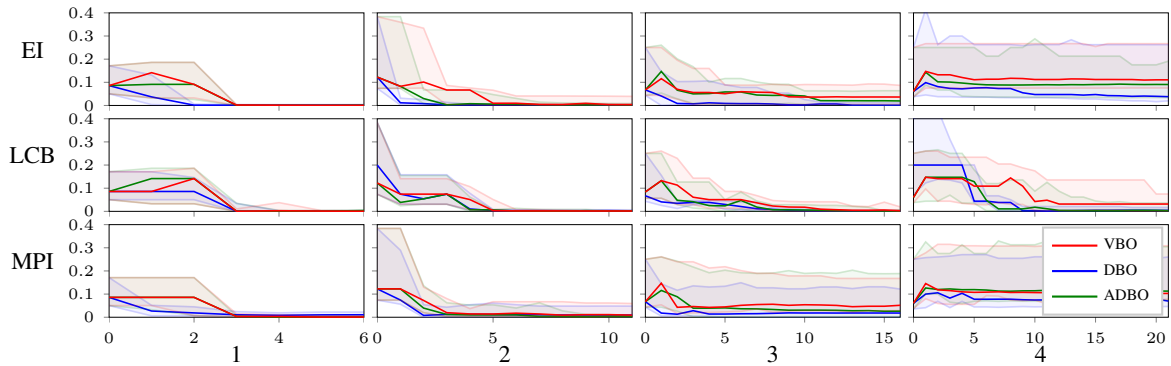


Figure 11: Same as in Figure 10, but with Sigopt functions are corrupted with noise of level $s = 0.05$.

Case Study 4: Simple Gaussian Functions With Minima on Border

Figures 12 and 13 illustrate the results for $s = 0$ and $s = 0.05$ introduced in the Section 4.4 of the main document.

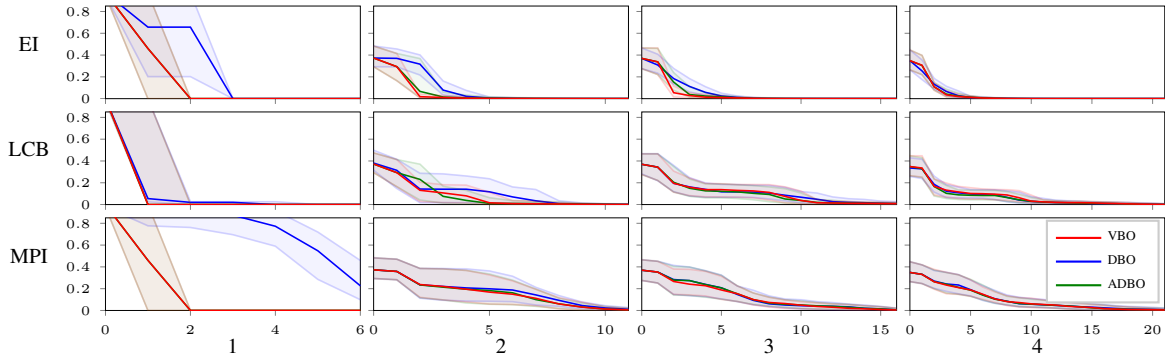


Figure 12: Same as in Figure 8, but with MND-functions that have local minimum on the edge of the search space.

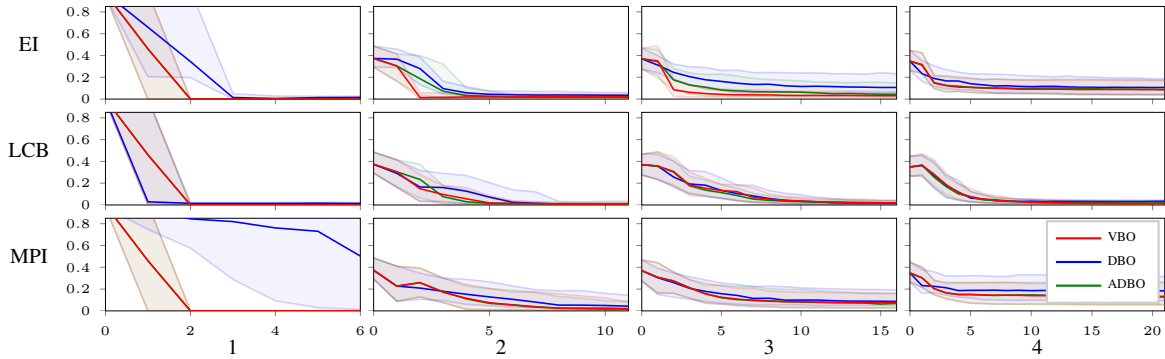


Figure 13: Same as in Figure 12, but MND-functions are corrupted with noise of level $s = 0.05$.